Journal of Vacuum Science and Technology A

RESEARCH ARTICLE | MARCH 24 2023

# Low-temperature synthesis of crystalline vanadium oxide films using oxygen plasmas

Brian Willis ; Adnan Mohammad ; Krishna D. Joshi ; Dhan Rana ; Saidjafarzoda Ilhom; Barrett Wells ; ; Boris Sinkovic; A. K. Okyay ; Necmi Biyikli



*J. Vac. Sci. Technol. A* 41, 032405 (2023)
https://doi.org/10.1116/6.0002383

JVST A
Journal of Vacuum Science & Technology A

ARTICLE

avs.scitation.org/journal/jva

# Low-temperature synthesis of crystalline vanadium oxide films using oxygen plasmas

Cite as: J. Vac. Sci. Technol. A 41, 032405 (2023); doi: 10.1116/6.0002383 Submitted: 28 November 2022 · Accepted: 23 February 2023 ·

Published Online: 24 March 2023

View Online Export Citation CrossMark

Adnan Mohammad,[1] Krishna D. Joshi,[2] Dhan Rana,[2] Saidjafarzoda Ilhom,[1] Barrett Wells,[2] Brian Willis,[3] Boris Sinkovic,[2] A. K. Okyay,[4,5] and Necmi Biyikli[1,a)]

AFFILIATIONS [1] Department of Electrical and Computer Engineering, University of Connecticut, Storrs, Connecticut 06269 [2] Department of Physics, University of Connecticut, Storrs, Connecticut 06269 [3] Department of Chemical and Biomolecular Engineering, University of Connecticut, Storrs, Connecticut 06269 [4] Department of Electrical Engineering, Stanford University, Stanford, California 94305 [5] OkyayTechALD LLC, Ankara 06374, Turkey

[a)]Author to whom correspondence should be addressed: necmi.biyikli@uconn.edu



## ABSTRACT

Vanadium oxide ($VO_x$) compounds feature various polymorphs, including $V_2O_5$ and $VO_2$, with attractive temperature-tunable optical and electrical properties. However, to achieve the desired material property, high-temperature post-deposition annealing of as-grown $VO_x$ films is mostly needed, limiting its use for low-temperature compatible substrates and processes. Herein, we report on the low-temperature hollow cathode plasma-enhanced atomic layer deposition (ALD) of crystalline vanadium oxide thin films using tetrakis(ethylmethylamido) vanadium and oxygen plasma as a precursor and coreactant, respectively. To extract the impact of the type of plasma source, $VO_x$ samples were also synthesized in an inductively coupled plasma-enhanced ALD reactor. Moreover, we have incorporated in situ Ar-plasma and ex situ thermal annealing to investigate the tunability of $VO_x$ structural properties. Our findings confirm that both plasma-ALD techniques were able to synthesize as-grown polycrystalline $V_2O_5$ films at 150 °C. Postdeposition thermal annealing converted the as-grown $V_2O_5$ films into different crystalline $VO_x$ states: $V_2O_3$, $V_4O_9$, and $VO_2$. The last one, $VO_2$ is particularly interesting as a phase-change material, and the metal-insulator transition around 70 °C has been confirmed using temperature-dependent x-ray diffraction and resistivity measurements.



## I. INTRODUCTION

Atomic layer deposition (ALD) is an emerging lowtemperature chemical vapor deposition technique, where the growth mechanism is based on the self-limiting gas-solid surface reactions.[1] It has several significant features when compared with other thin film deposition processes: low temperature deposition, atomic scale thickness control, large-area uniformity, 3D conformality, and pinhole-free dense films.[2] The plasma-enhanced atomic layer deposition (PEALD) technique has additional benefits compared to the conventional thermal-ALD. The plasma-generated highly reactive radicals enable the surface ligand exchange reactions to happen more effectively at lower substrate temperatures. These features make it possible to fabricate and process a wide variety of compound films at CMOS-compatible temperatures and on temperature-sensitive flexible substrates like polymer or organic surfaces.[3–9] ALD has also started contributing to solar cells,[10,11] energy storage,[12–14] nanocatalysis,[15–17] passivation,[18,19] and wearable devices.[20–22] $VO_x$ is an attractive compound material family featuring a wide spectrum of applications. Vanadium pentoxide ($V_2O_5$) is used in implantable medical devices-rechargeable batteries, photovoltaic applications, nanowires, nanofibers,[23,24] super capacitors,[25–30] electrochromic devices,[31–33] etc. On the other hand, vanadium dioxide ($VO_2$) shows metal-to-insulator transition (MIT) at a relatively low temperature (~70 °C) and can be utilized in

electrical/RF and optical switches,[34,35] chromogenics,[36,37] and modulator and memory devices.[38,39]

A relatively limited number of studies have been reported in the literature on $VO_x$ growth using thermal and plasma-enhanced ALD. The vast majority of low-temperature $VO_x$ synthesis studies are carried out via thermal ALD, mostly resulting in an as-grown amorphous film. Most of the reports followed a postdeposition annealing process to crystallize the films. Table I shows the reported studies on ALD grown $VO_X$ films.

TABLE I. Reported studies on ALD grown $VO_x$.

| Reported by | ALD type | Precursor | Coreactant | As-grown film properties | Substrate temperature (°C) | Annealing condition | |
|---|---|---|---|---|---|---|---|
| Premkumar et al.[40] | Thermal | TEMAV | Ozone | Amorphous | 150 | 425–500 °C | $N_2$ and $O_2$ |
| Wang et al.[41] | Thermal | TDMAV | Ozone/water | Amorphous | 50–200 | 550–600 °C | $N_2$ |
| Prasadman et al.[42] | Thermal | VTOP | Water | Amorphous | 80 | 550 and 700 °C | Vacuum |
| Musschoot et al.[43] | Thermal and ICP-ALD | VTIP | Water, water and oxygen plasma | Amorphous and crystalline | 150 | 400–500 °C | $O_2$ |
| Kazadojev[44] | ICP-ALD | TDMAV | $O_2$/Ar plasma | Crystalline | 250 | 400 °C | Air |

Besides having very few reports on PEALD of $VO_x$ thin films,[43,44] only inductively coupled plasma-ALD (ICP-ALD) has been reported while other remote plasma configurations are significantly missing. In this work, a detailed investigation of hollowcathode plasma-ALD (HCP-ALD) of $VO_x$ thin films at 150 °C substrate temperature is performed, analyzed, and compared to ICP-ALD. The vanadium oxide thin films are grown using TEMAV precursor and oxygen ($O_2$) plasma as a coreactant. The as-grown films are also treated under postdeposition annealing processes in a high-vacuum customized PLD reactor to observe annealingdependent transformation of the $VO_x$ crystal structure. An additional in situ plasma processing step, in situ Ar-plasma annealing, was incorporated in the HCP-ALD unit cycle to see if the crystalline phase change toward the sought-after $VO_2$ phase would have been possible without the need for high-temperature postdeposition annealing.

## II. EXPERIMENTAL DETAILS

In this section, the ICP-ALD and HCP-ALD reactors and recipes for $VO_x$ growth are discussed as well as the postdeposition and ex situ annealing processes carried out. The film characterization methods and details used in this work to define the structural, optical, and electrical film properties are explained.

### A. Film growth

Veeco/Ultratech Fiji-200 G2.0 ICP-ALD (Veeco Inc., NY) and OKYAYTECHALD P100 HCP-ALD (OkyayTech Ltd., Ankara, Turkey) reactors are used for film deposition experiments. The OKYAYTECHALD reactor is integrated with an FS-1 multiwavelength ellipsometer (FilmSense LLC, NE) to record the real-time optical thickness variation during the film growth process. A pulsed-laser deposition (PLD) chamber (PVD Products Inc., MA) is used for ex situ or postdeposition annealing purpose. We have used bare Si(100) and $Al_2O_3$ (HCP-ALD grown) coated Si(100) as substrates. The Si(100) substrate went through a conventional substrate surface cleaning process (acetone, isopropyl alcohol, and DI water). Then, the samples were $N_2$ dried before loading into the reactor. The chamber base pressure was ~155 mTorr, and the substrate temperature is varied between 100 and 250 °C. Tetrakis(ethylmethylamido) vanadium (TEMAV) is used as V precursor and $O_2$-only or $O_2$/Ar plasma as the oxygen coreactant, respectively. In addition, the TEMAV precursor was heated at 115 °C in order to provide a sufficient amount of precursor vapor into the reactor chamber. Precursor pulsing times are kept fixed at 100 ms during the experiments in ICP-ALD and at 240 ms in HCP-ALD experiments. The plasma parameters are kept fixed at 100 W in ICP-ALD with 50 SCCM $O_2$-only plasma, while in HCP-ALD at 100 and 150 W with 50 SCCM $O_2$-only and 50/20 SCCM and $O_2$/Ar plasma. Ar was used as purge gas: 20 SCCM in ICP-ALD and 50 SCCM in HCP-ALD. As carrier gas flow, 20 SCCM Ar is used in the ICP-ALD reactor and 10 SCCM $N_2$ in the HCP-ALD reactor. HCP-ALD reactor is used for Ar-plasma in situ annealing at 20 s, 20 SCCM Ar plasma within the rf-power range of 50–200 W. A typical unit cycle PEALD recipe for $VO_x$ thin film growth and in situ plasma annealing is depicted in Fig. 1. The in situ plasma annealing step is added to the unit ALD cycle just after the completion of the conventional PEALD cycle.



A customized PLD chamber is used for ex situ thermal annealing. The air-exposed and as-received films are annealed at a temperature range 450–700 °C and under $10^{-3}$ to 1 mTorr pressure controlled with $O_2$ flow.

### B. Film characterization

#### 1.Insitucharacterization

In situ ellipsometry is used to record the real-time film thickness variation and to obtain insight into the individual surface reactions (precursor chemisorption and ligand removal/exchange reactions). It is possible to observe, compare, and analyze the surface reactions during each ALD cycle due to the subangstrom resolution of the ellipsometer. The FS-1 multiwavelength ellipsometer (MWE) unit (Film Sense LLC, NE) is used to monitor the realtime film growth process. The ellipsometer uses blue, green, yellow, and red-light

emitting diodes (LEDs) as the source of illumination. A uniform beam is developed within the source unit and fed into the detector unit after reflecting from the sample surface. The fitting model used for the ellipsometry measurement data is Cauchy/$SiO_2$(native)/Si. The growth per cycle (GPC) is calculated by averaging the thickness gain over a number of ALD cycles.

2.Exsitucharacterization

The multiwavelength ellipsometer (MWE) unit is used for ex situ characterizations on its ex situ measurement base to obtain the optical constants of the films. Grazing-incidence x-ray diffraction (GIXRD) and reflectivity (XRR) measurements are performed by a Rigaku SmartLab multipurpose x-ray diffractometer (Rigaku Corporation, Japan) operated at 45 kV and 40 mA by using Cu Kα radiation. The x-ray source is set fixed at ω = 0.3° and w at 30°, while the detector position (2θ) is changed between 10° and 70°. For elemental composition, chemical bonding states, and impurity incorporation analysis, x-ray photoelectron spectroscopy (XPS) measurements are performed using a monochromatic Al Kα x-ray (1486.6 eV) source and a Scienta SES-100 electron analyzer. The film surface images are captured by a Helios Nanolab 460F1 dualbeam focused-ion beam scanning electron microscope (FIB/SEM) (Thermo Fisher Scientific, USA) to analyze the surface morphologies. A customized home-built Hall measurement setup

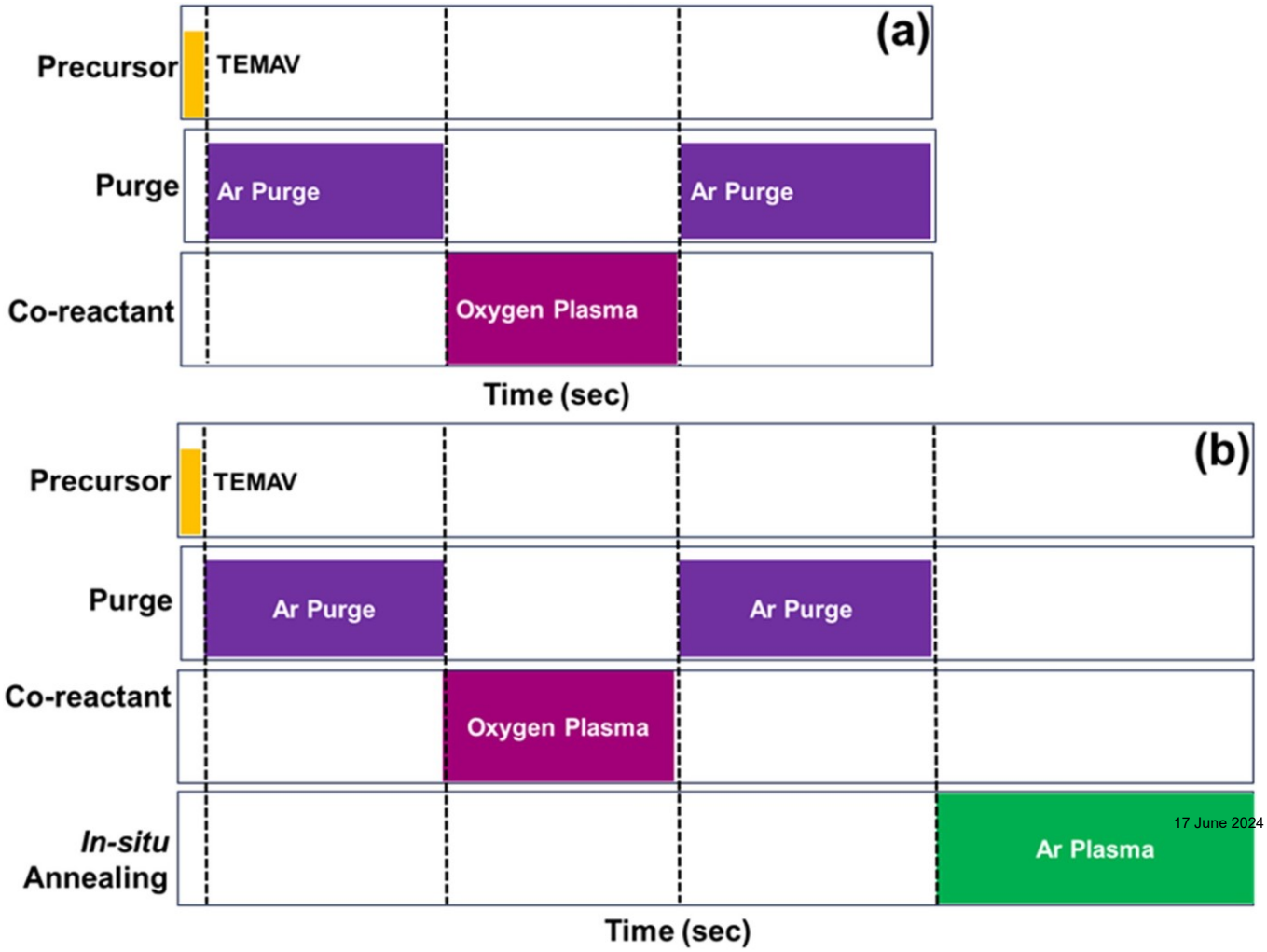


FIG. 1. Time-domain evolution of the (a) unit-cycle plasma enhanced atomic layer deposition (PEALD) process of $VO_x$ thin film and (b) in situ plasma annealing incorporated PEALD cycle.

with a semiconductor parameter analyzer is used for temperature dependent resistivity measurements.

## III. RESULTS AND DISCUSSION

In this section, the film growth process, optical, structural, and chemical properties of the $VO_x$ samples grown via ICP-ALD and HCP-ALD and postdeposition annealing characteristics will be discussed.

### A. ICP-ALD grown vanadium oxide ($VO_x$) thin films

Table II shows the measured film thickness, GPC, and refractive index values for the ICP-ALD grown $VO_x$ thin films at two different rf-plasma powers of 100 and 300 W. The refractive index values are relatively close (2.50 vs 2.55 Å) as well as the GPC results (0.59 vs 0.64 Å). The refractive index values found for ICP-ALD grown $VO_x$ are in close agreement with prior reports.[45] As the GPC and optical refractive index values are similar at both 100 and 300 W, the 100 W recipe is chosen as the preferred rf-plasma power value for ICP-ALD grown $VO_x$.

TABLE II. Measured refractive index and growth per cycle (GPC) values of the 300 cycle ICP-ALD grown $VO_x$ thin films on Si (100) at 150 °C.

| Plasma power (W) | Thickness (nm) | GPC (Å) | Refractive index (n) |
|---|---|---|---|
| 100 | 19.3 | 0.64 | 2.55 |
| 300 | 17.9 | 0.59 | 2.50 |

The GIXRD scans of the as-grown $VO_x$ thin film samples on Si(100) substrates are shown in Fig. 2. The relatively close result confirms that both rf-plasma power values are sufficient to achieve as-grown crystalline $V_2O_5$ films with a strong (001) peak and a weaker (101) signal. Hence, in terms of the diffraction peak intensity and crystalline orientation, the 100 W recipe can be accounted for as the best growth recipe in this study.

Figure 3 shows the crystallinity transformation of the ICP-ALD grown $V_2O_5$ thin films by postdeposition annealing with respect to annealing pressure: $10^{-3}$ mTorr (no $O_2$ flow), 0.1, 0.5, and 1 mTorr $O_2$ ambient, while the annealing temperature is fixed at 600 °C. At 600 °C, the $V_2O_5$ state loses its stability[46] and converts to $V_2O_3$ with (012), (104), (110), and (113) diffraction peak orientation under $10^{-3}$ mTorr pressure (base vacuum level). An increase in annealing chamber pressure to 0.1 mTorr $O_2$ flow keeps the same $V_2O_3$ diffraction peaks with an increase in the peak intensity. However, the oxygen incorporation increases and transforms to $VO_2$ (011) state for both 0.5 and 1 mTorr chamber pressure values. Hence, we can conclude that at higher

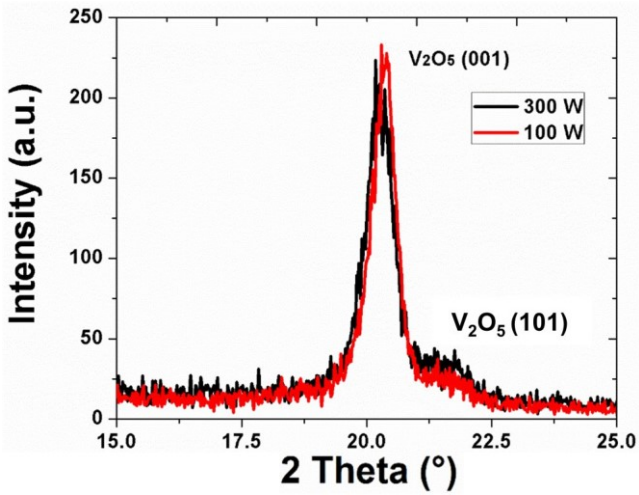


FIG. 2. GIXRD of the 300 cycle as-grown $VO_x$ thin films on Si(100) in an ICP-ALD reactor at 150 °C using 100 and 300 W rf-plasma power. The dominant diffraction peak matches with the (001) orientation of $V_2O_5$.

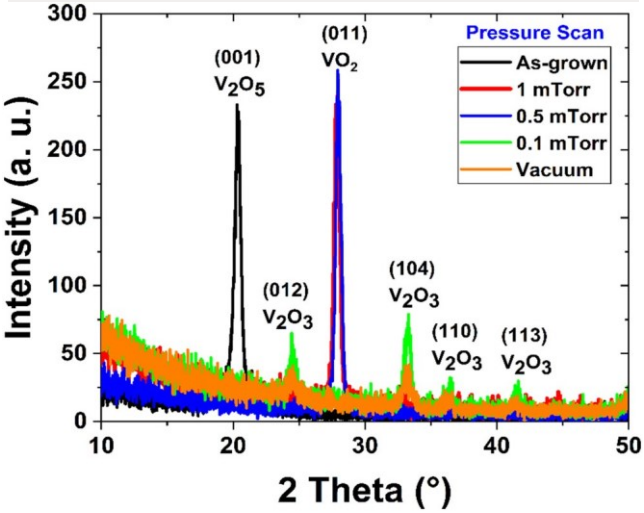


FIG. 3. GIXRD of the ICP-ALD as-grown $V_2O_5$ film and postdeposition annealed $VO_2$ thin film samples showing the impact of annealing $O_2$ pressure, varied from $10^{-3}$ to 1 mTorr at 600 °C for 30 min.

annealing temperatures where $V_2O_5$ state becomes unstable, controlled low-pressure $O_2$ flows result in different $VO_x$ stoichiometries with reduced O/V ratio. The best $O_2$ flow for 2 5

ICP-ALD grown $V_2O_5$ thin films under 0.5 mTorr $O_2$ ambient is shown in Fig. 4. The O/V ratio is reduced with increasing



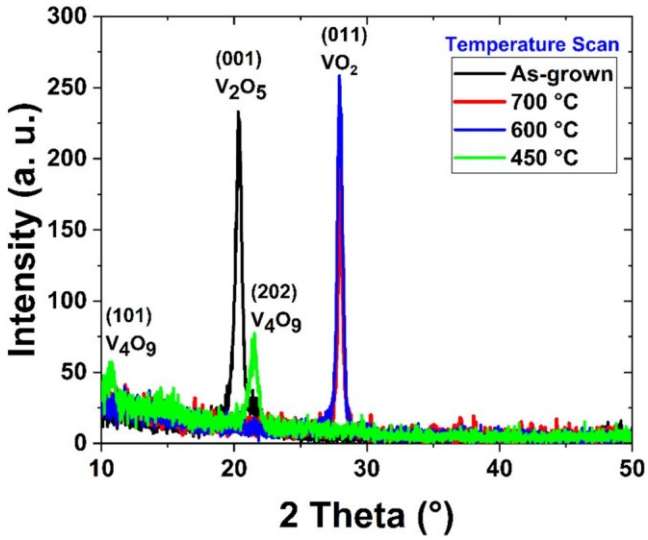


transforming the as-grown V O phase into the desired $VO_2$ phase is found as 0.5 mTorr.

The influence of postdeposition annealing temperature on

FIG. 4. GIXRD of the ICP-ALD as-grown and postdeposition annealed $VO_x$ films showing the impact of annealing temperature within 450–700 °C at a fixed pressure of 0.5 mTorr $O_2$ ambient for 30 min.

annealing temperature, and at 450 °C, the resulting material phase is $V_4O_9$ with (101) and (202) diffraction peaks. As the annealing temperature increases to 600 °C, the O/V ratio gets further reduced and stabilized at ~2.0, displaying the $VO_2$ state. The $VO_2$ phase is preserved at 700 °C as well under 0.5 mTorr chamber pressure.

$VO_2$ is a bistate material that shows a crystalline phase transition at low temperatures from the monoclinic to tetragonal crystal phase. As shown from the temperature-dependent GIXRD scan in Fig. 5, the $VO_2$(011) monoclinic phase is observed at a temperature ranging from room temperature to 60 °C. Around 70 °C, the phase-transition from monoclinic to tetragonal phase takes place, which is parallel to prior reports.[47] The $VO_2$(110) tetragonal phase sustains itself at higher ambient temperatures up to at least 110 °C.

Figures 6(a) and 6(b) show the top-view high-resolution SEM image of the ICP-ALD grown $V_2O_5$ and postdeposition annealed $VO_2$ thin films, respectively. The as-grown 26 nm-thick $V_2O_5$ film looks relatively uniform with certain density of voids. On the other hand, the annealed $VO_2$ film shows discontinuity and agglomeration of islands reflecting the impact of the postdeposition annealing process. As will be discussed for HCP-ALD grown $VO_x$ samples, the voids in the as-grown films and discontinuous island characteristics in the annealed $VO_2$ films can be potentially compensated by further increasing the thickness of $VO_x$ films.

The measured and calculated XRR of ICP-ALD grown $V_2O_5$ is shown in Fig. 7(a). The model used to calculate and fit the XRR pattern is $V_2O_5/SiO_2/Si$, which gives a good fit and reveals that the film density is ~3.15 g $cm^{-3}$ which is reasonably close to the reported bulk value of 3.36 g $cm^{-3}$.[48,49] The data fitting revealed a film thickness of ~33 nm, which is slightly thicker than our ellipsometry-measured values, and the film surface roughness of ~1.7 nm was calculated. A similar fitting approach for $VO_2$ film is performed using $VO_2/SiO_2/Si$ model and the XRR pattern is displayed in Fig. 7(b). The calculated thickness, density, and roughness are ~20 nm, 4.03 g/$cm^3$, and 5.90 nm respectively. The calculated thickness value is close to the ellipsometry-measured thickness value. The density found is smaller than the reported bulk density value of 4.57 g/$cm^3$.[49] However, the higher roughness is attributed to the discontinuity of $VO_2$ film triggered by the postdeposition annealing, which can be overcome by growing thicker films as will be demonstrated with the HCP-ALD grown and postdeposition annealed samples.

Figure 8 shows the elemental content and atomic concentrations of the ICP-ALD grown $V_2O_5$ film for air-exposed as-received samples without any Ar sputtering, extracted via XPS measurements from the surface of the samples. The O/V ratio for the film is ~2.4, which is rather close to the ideal stoichiometric ratio (2.5) of $V_2O_5$ films. The carbon content is ~23% and originates mainly from the surface XPS measurement where atmospheric contamination results

typically in higher carbon concentration. The existence of nitrogen is ~5% and mainly resulting from the nitrogencontaining TEMAV, $[(C_2H_5)(CH_3)N]_4V$ precursor itself. This result indicated that the ICP-ALD $O_2$-only plasma recipe was probably not sufficient to completely remove the nitrogen containing ligands during $O_2$-plasma cycles.

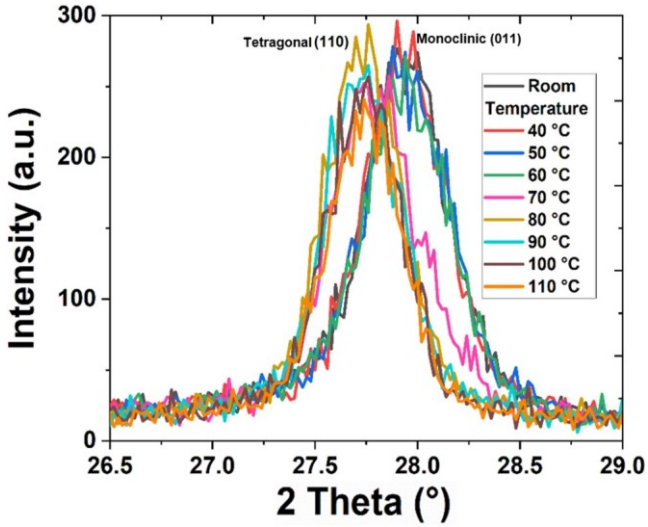


FIG. 5. Temperature-dependent GIXRD measurement of the postdeposition annealed $VO_2$ thin film showing crystalline phase transition from monoclinic to tetragonal at ~70 °C, confirming the metal-insulator transition behavior of $VO_2$.
The temperature scan is performed from room temperature to 110 °C.

Before going into the details of the HCP-ALD grown VOx films and their material properties, we would like to note that the HCP-ALD reactor possessed the in situ growth process monitoring capability with its integrated multi-wavelength ellipsometry. Therefore, HCP-ALD grown $VO_x$ sample results will include a study of the film growth process and unit-ALD cycle behavior analysis, which reveals additional insight and knowledge about the surface growth reactions.

The in situ ellipsometry recorded 300 cycles and unit ALD cycle thickness data of HCP-ALD grown $VO_x$ thin films at 150 °C and 100 W plasma are shown in Figs. 9(a) and 9(b), respectively. Figure 9(a) shows that the $VO_x$ thickness gain at 300th cycle with 50 and 10 SCCM $O_2$ plasma is ~47 and ~28 nm, respectively. The higher $O_2$ flow during plasma-assisted ligand removal process produces more energetic O* radicals that leads to more efficient TEMAV chemisorption in the following ALD cycle. Hence, the TEMAV chemisorption with 50 SCCM $O_2$ plasma is recorded as ~0.90 nm and higher if compared with the TEMAV chemisorption of ~0.65 nm under 10 SCCM $O_2$ plasma as evident from Fig. 9(b). Likewise, the GPC increases from ~0.09 nm (at 10 SCCM) to ~0.15 nm (at 50 SCCM).

Table III shows the thickness, GPC, and refractive index values of the 600 cycle HCP-ALD grown $VO_x$ thin films under different plasma chemistries and durations extracted from the ex

### B. HCP-ALD grown $VO_x$ thin films

situ ellipsometry. The substrate temperature and plasma power were kept fixed at 150 °C and 100 W, respectively. The film grown with 50 SCCM $O_2$-only plasma at 10 s shows the highest

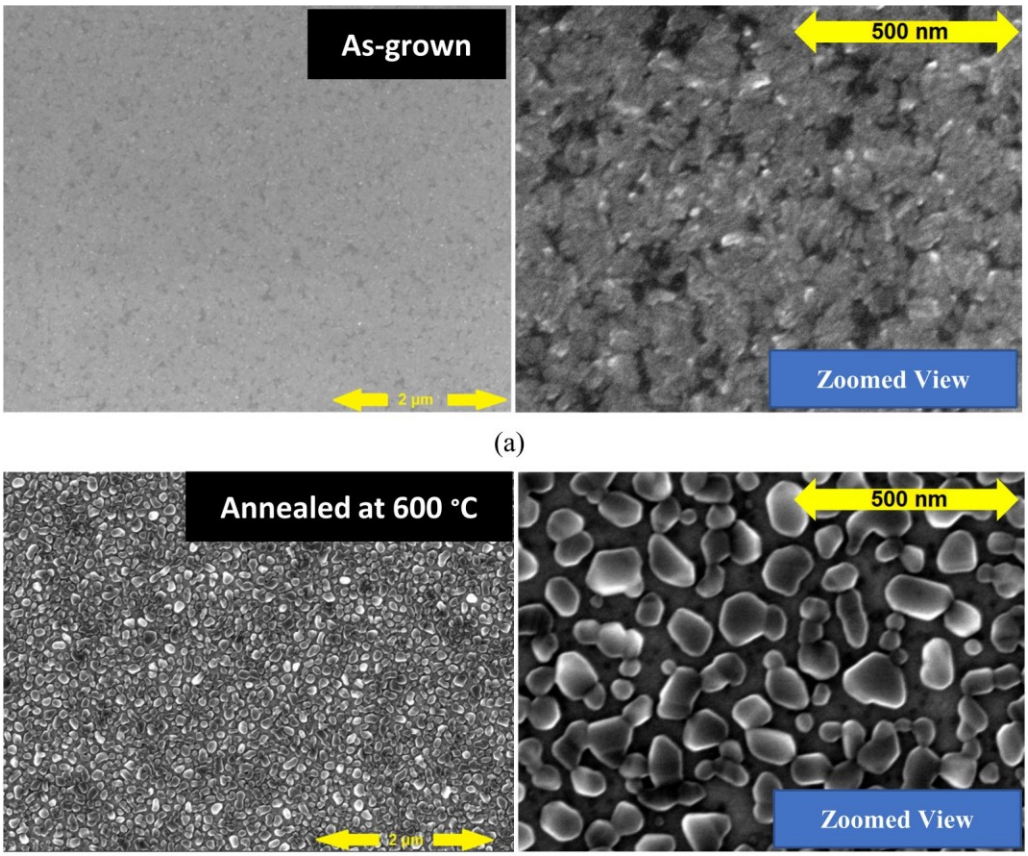


FIG. 6. Top-view HR-SEM and comparative morphological change of (a) ~26 nm thick ICP-ALD as-grown $V_2O_5$ film and (b) ~25 nm thick annealed postdeposition (600 °C, 0.5 mTorr $O_2$ ambient) $VO_2$ thin film.

GPC value of 1.80 Å and a refractive index of 2.76. The GPC and refractive index both decrease to 1.25 Å and 2.33 respectively at 10 SCCM $O_2$ plasma. We can attribute the decrease in GPC and refractive index value to the insufficient ligand removal process as the density of plasma-generated reactive O* radicals reduces with decreasing $O_2$ flow from 50 to 10 SCCM. Next, an increase in the plasma duration to 20 s at 10 SCCM $O_2$ plasma resulted in an increase in the refractive index to 2.61, while the GPC reduced to 0.8 Å. As we provided longer plasma duration for ligand removal process, the refractive index increased, and GPC was reduced accordingly. When comparing the film properties between Ar/$O_2$ 20/50 and 50 SCCM $O_2$-only plasma grown $VO_x$ films, one can conclude that both GPC and refractive index reduce to 1.3 Å and 2.60. Lastly, the addition of 20 s, 100 W, 20 SCCM Ar-plasma in situ annealing in the conventional 10 s, 50 SCCM $O_2$ plasma $VO_x$ recipe has slowed down the GPC to 0.83 Å most possibly due to the more effective removal of the chemisorbed and physiosorbed surface groups with a slight reduction in the refractive index from 2.76 to 2.70.

Figure 10 compares the GIXRD scans of the $VO_x$ thin film samples grown via ICP-ALD and HCP-ALD reactors at 150 °C. The plasma parameters are 100 W, 10 s of 50 SCCM $O_2$-only flow. The resulting as-grown film is $V_2O_5$ with a dominant (001) and much weaker (101) shoulder peak. Hence, we conclude that both ICP-ALD and HCP-ALD techniques lead to as-grown crystalline vanadium pentoxide ($V_2O_5$) phase films. Using the Scherrer equation, $D = 0.9\lambda/d(\cos\theta)$, where D is the average grain size, λ is the x-ray wavelength, d is the full-width-at-half-maximum (FWHM) of the XRD peak in radians, and θ is the angle in degree the average crystal grain sizes are found. The grain sizes for the HCP-ALD and ICP-ALD grown $V_2O_5$ film are calculated as ~15.5 and 13.5 nm.

The GIXRD of $VO_x$ films grown at 100 and 150 W rf-plasma power in the HCP-ALD reactor are shown in Fig. 11(a). Both

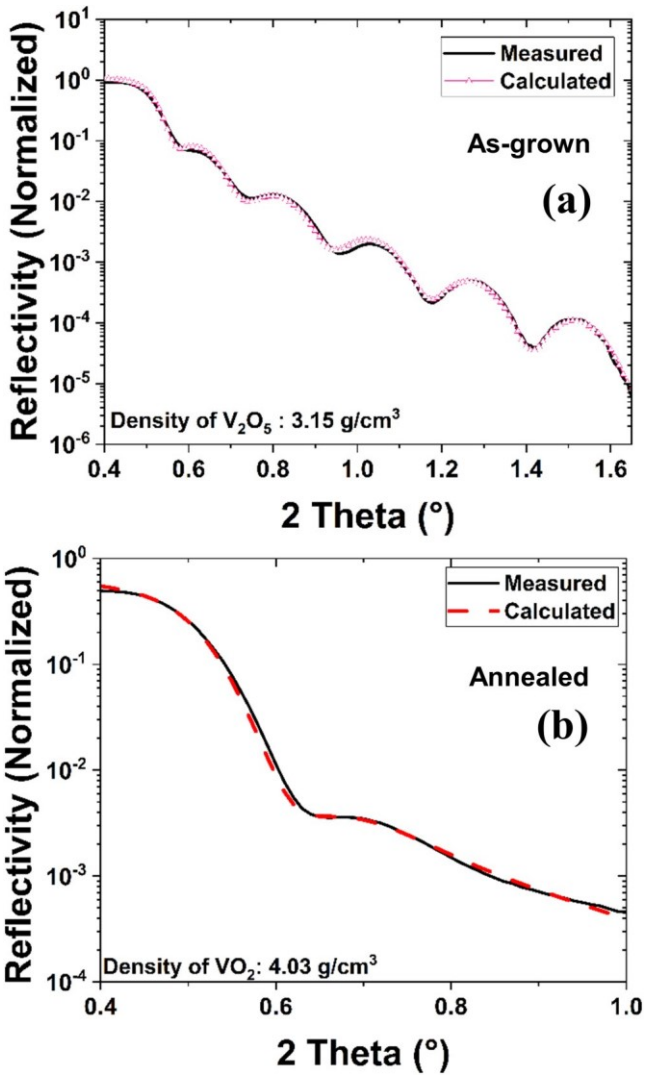


FIG. 7. XRR analysis of (a) as-grown $V_2O_5$ thin film via ICP-ALD 450 cycles and (b) $VO_2$ film obtained after postdeposition annealing at 600 °C, 0.5 mTorr $O_2$ pressure.

samples showed $V_2O_5$ films with a (001) dominant peak. The impact of plasma chemistry on the film crystallinity of HCP-ALD grown $VO_x$ thin film is depicted in Fig. 11(b). However, similar to $V_2O_5$ diffraction peaks, the (001) peak intensity for the $O_2$/Ar plasma samples is lower compared to the $O_2$-only plasma grown $VO_x$ film, partly due to the film thickness difference as outlined by Table III (see Fig. S1 in the supplementary material).[55]

The GIXRD scans of as-grown $VO_x$ samples via HCP-ALD at different substrate temperatures (100, 150, 200, and 250 °C) are shown in Fig. 11(c). However, the $V_2O_5$ phase with dominant

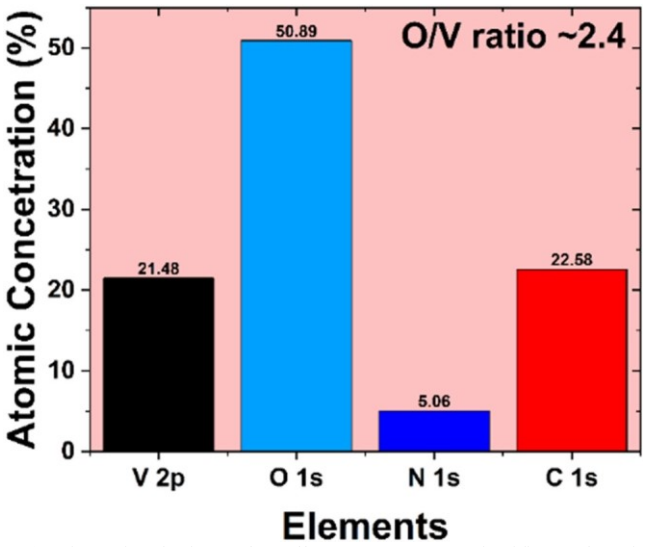


(001) orientation is formed at all temperatures, a significant drop in the diffraction peak intensity is observed at higher growth

FIG. 8. Elemental content (V, O, N, C) of the ICP-ALD grown $V_2O_5$ thin film grown with ICP-ALD at 100 W $O_2$ plasma, 150 °C for 300 cycles, revealing a near-ideal O/V stoichiometry value of ~2.4.

temperatures (200–250 °C) possibly due to reduced GPC and resulting film thickness values (see Fig. S2 in the supplementary material).[55] Figure 11(d) shows how the GIXRD scan changes with the additional in situ Ar-plasma annealing in the HCP-ALD reactor. The samples were Ar-annealed for 20 s at 50, 100, 150, and 200 W plasma power. Although all in situ Ar-plasma annealing experiments have resulted in $V_2O_5$ films, the one at 100 W is showing maximum diffraction peak intensity and is close to the diffraction peak intensity of the as-grown $V_2O_5$ film. Within the experimented conditions, we have confirmed that in situ Ar-plasma annealing was not able to transform the $VO_x$ crystal phase from $V_2O_5$ into the targeted $VO_2$ phase. While Kao et al. reported significant improvement of the AlN crystal quality by the means of layer-by-layer in situ plasma annealing at a low temperature below 300 °C.[50] Therefore, ex situ postdeposition annealing experiments were carried out.



The phase transformation of the HCP-ALD grown $V_2O_5$ films to $VO_2$ by postdeposition annealing is shown in Fig. 12 and Table IV. The samples are grown in the HCP-ALD reactor with four different recipes: 100 W–50 SCCM $O_2$-only plasma at (i) 150 °C, (ii) 100 °C, (iii) 150 °C, 100 W, 10 SCCM $O_2$-only, and (iv) 150 °C, 100 W, 20/50 SCCM Ar/$O_2$ plasma recipe. These selected samples are annealed at 500 and 600 °C under 0.5 mTorr $O_2$ pressure. However, both annealing temperatures have successfully converted the as-grown $V_2O_5$ films to $VO_2$, the 600 °C annealing temperature reduces the intensity of diffraction peaks as displayed in Fig. 12. Hence, 500

°C is the best annealing temperature as it provides a stronger $VO_2$(011) diffraction peak intensity.

The temperature dependent GIXRD scans for the postdeposition annealed HCP-ALD grown $VO_2$ samples are shown in Fig. 13.

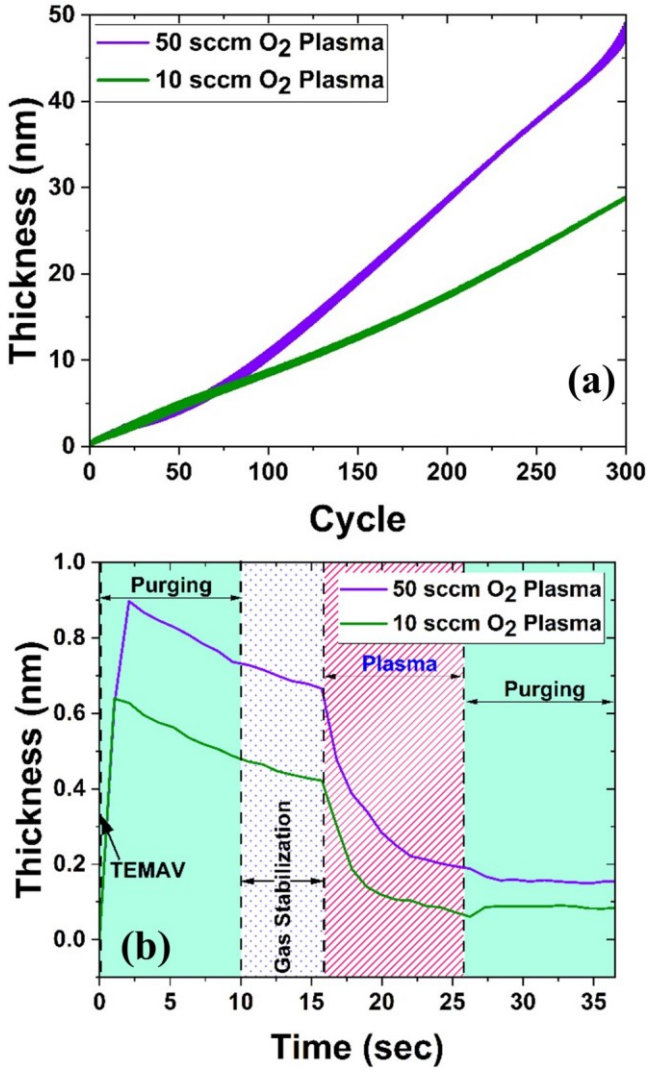


FIG. 9. In situ ellipsometry monitored growth evolution for HCP-ALD grown $VO_x$ thin films at 150 °C substrate temperature. (a) 300 ALD cycles showing the film growth behavior, and (b) average unit ALD cycle data as a function of 10 and 50 SCCM $O_2$ flow during the 100 W plasma exposure period.

TABLE III. Measured refractive index and growth per cycle (GPC) values of the 600 cycles HCP-ALD grown VOx thin films on Si(100) at 150 °C and 100 W plasma power under different plasma conditions.

| Sl | Plasma chemistries and duration | Thickness (nm) | GPC (Å) | Refractive index |
|---|---|---|---|---|
| 1 | 50 SCCM $O_2$ for 10 s | 108 | 1.80 | 2.76 |
| 2 | 10 SCCM $O_2$ for 10 s | 75 | 1.25 | 2.33 |
| 3 | 10 SCCM $O_2$ for 20 s | 48 | 0.80 | 2.61 |
| 4 | Ar/$O_2$ 20/50 SCCM for 10 s | 78 | 1.30 | 2.60 |
| 5 | 50 SCCM $O_2$ for 10 s + in situ annealing | 50 | 0.83 | 2.70 |

FIG. 10. Comparing film crystallinity of the $VO_x$ thin film samples grown via HCP-ALD and ICP-ALD using 100 W rf-plasma power for 10 s with 50 SCCM $O_2$-only flow at 150 °C substrate temperature.

The temperature range for this scan is room temperature to 100 °C. The monoclinic to tetragonal $VO_2$ phase transition is observed at 70 °C. The $VO_2$ (110) tetragonal phase sustains at 100 °C. Hence, this temperature scan has successfully verified the mentalinsulator phase transition (MIT) properties of the $VO_2$ thin film.

The film surface morphologies of the HCP-ALD grown $V_2O_5$ and ex situ annealed $VO_2$ films are illustrated in Fig. 14. The as-grown $V_2O_5$ film with a recipe of 100 W, 50 SCCM $O_2$-only plasma via HCP-ALD looks uniform and void-free as displayed in Fig. 14(a). The 600 °C annealed $VO_2$ film (as-grown $V_2O_5$ via 50 SCCM $O_2$-only plasma) surface is depicted in Fig. 14(b). While annealing successfully converted the film phase to the $VO_2$ state, voids are formed due to higher temperature annealing and crystal transformation as a result of thermal annealing. Also, as the HCP-ALD grown film is thicker (~108 nm), the discontinuity among the annealed film grains is diminished compared to the thinner (~26 nm) annealed $VO_2$ film grown within the ICP-ALD reactor [Fig. 6(b)]. The SEM image of 500 and 600 °C annealed 10 SCCM $O_2$-only plasma HCP-ALD grown samples are shown in Figs. 14(c) and 14(d). In comparison with the 600 °C annealed film surface, the 500 °C annealed $VO_2$ film shows smaller crystalline grains due to reduced annealing temperature. Hence, the diffraction peak intensity in the GIXRD of 500 °C annealed $VO_2$ film (Fig. 12, sample "B") is maximum.

Figure 15 and Table V summarize the XRR measurement results for the HCP-ALD grown $VO_X$ thin films for the following recipes: (i) 10 s, $O_2$-only (10 SCCM) plasma, (ii) 20 s, $O_2$-only (10 SCCM) plasma, and (iii) 100 W, 20 s and 20 SCCM Ar-plasma in situ annealed $V_2O_5$ film (10 s, 50 SCCM $O_2$-only plasma). The $V_2O_5/SiO_2/Si$ layer structured model is used for calculation and fitting purposes. The 20 s $O_2$ plasma grown $V_2O_5$ sample showed a maximum film density of 3.19 g/cm$^3$ as longer plasma duration might lead to more effective ligand (carbon group) removal and, thus, improving the film density. The 10 s plasma grown $V_2O_5$ film has a notably lower film density of 2.85 g/cm$^3$. The film density variation as a function of $O_2$ plasma exposure time is in close agreement with the ex situ ellipsometry recorded refractive index values shown in Table III: 2.61 versus 2.33 for plasma durations of 20 and 10 s, respectively. No direct comparison can be made for the Ar-plasma in situ annealed $V_2O_5$ film as annealing is performed on the 10 s, 50 SCCM $O_2$-only plasma grown film, which resulted in a film density value of 3.07 g/cm$^3$. The roughness values found for the aforementioned films here are within 2–3 nm, while the ex situ ellipsometer measured thickness values for the $V_2O_5$ films are reasonably close to the XRR extracted thickness data. XRR-fitted data exhibit 10%–15% higher thickness values than the ellipsometer recorded values.

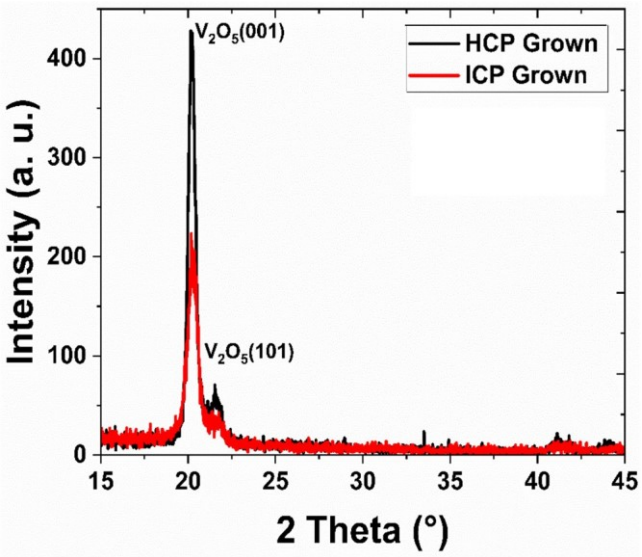


FIG. 11. Crystallinity analysis by GIXRD of the HCP-ALD grown $VO_x$ thin films as a function of (a) rf-plasma power (100 and 150 W), (b) plasma chemistry ($O_2$-only and $O_2$/Ar), (c) substrate temperature (100–250 °C), and (d) in situ Ar-plasma annealing.

Figure 16 shows the core level XPS spectrum of constituent elements, V and O, of the HCP-ALD grown film. The binding energy was calibrated using the adventitious carbon, C1s, at 284.8 eV as a reference. The spectrum was analyzed using the Gaussian–Lorentzian line shape for the peak fitting and Shirley function to subtract the background. The V 2p3/2 and V 2p1/2 peaks were found at 516.9 and 524.2 eV, respectively, which implies the vanadium atoms are in the $V^{5+}$ state, indicating the presence of $V_2O_5$. The O 1s peak position at 529.7 eV also indicates that oxygen and vanadium atoms are bound into $V_2O_5$, based on the O 1s binding energy reported in the literature.[51] The fitting of the V 2p peaks necessitates a small peak at lower binding energy of the $V^{5+}$ state suggesting the presence of a minority $V^{4+}$ state (amounting to 9% of total V). This small amount of $V^{4+}$ species is likely due to growth termination that resides at the surface of the film, hence not observable by other, bulk sensitive techniques. The pronounced shoulder at the higher binding energy of O 1s spectrum indicates the presence of an additional oxygen state, which we assign to the atmospheric contaminants since the films were exposed to air for many hours before the XPS measurement. This is confirmed by fitting the shoulder with two components assigned to –OH and water contaminants at 1.4 and 2.9 eV, respectively.[52,53] The elemental composition analysis indicates the ratio of V and O, bound to V, (V/O) to be ~2.5 which further supports formation of the $V_2O_5$ film.

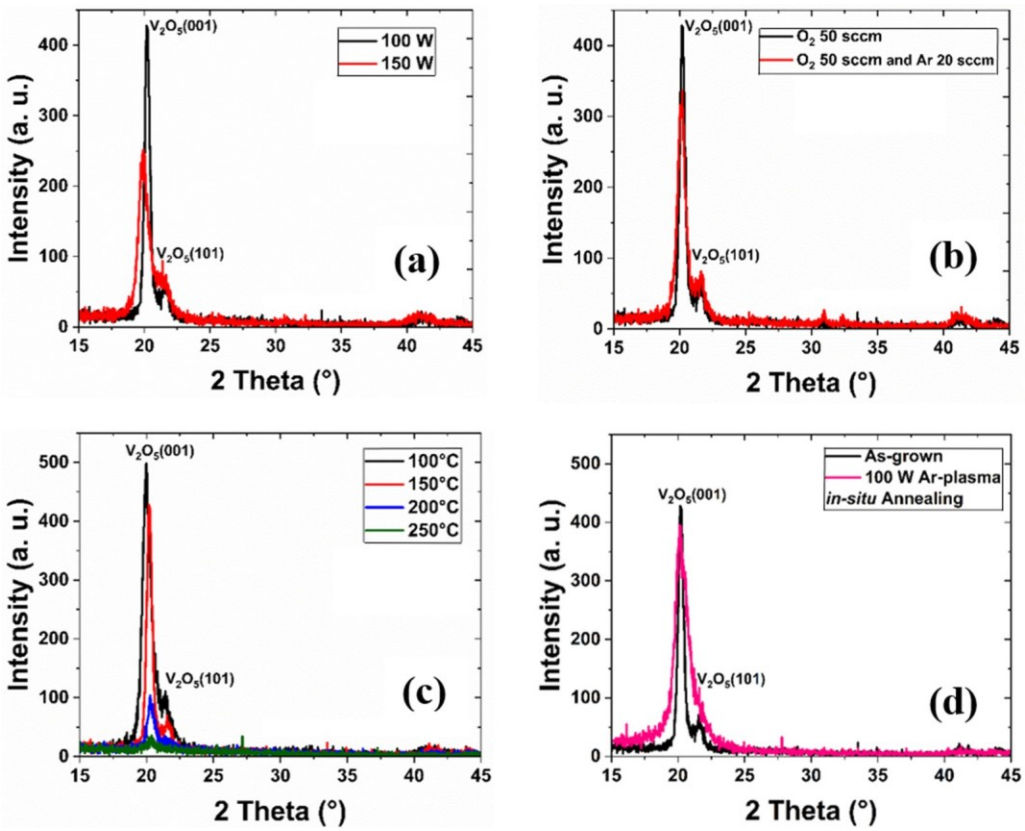

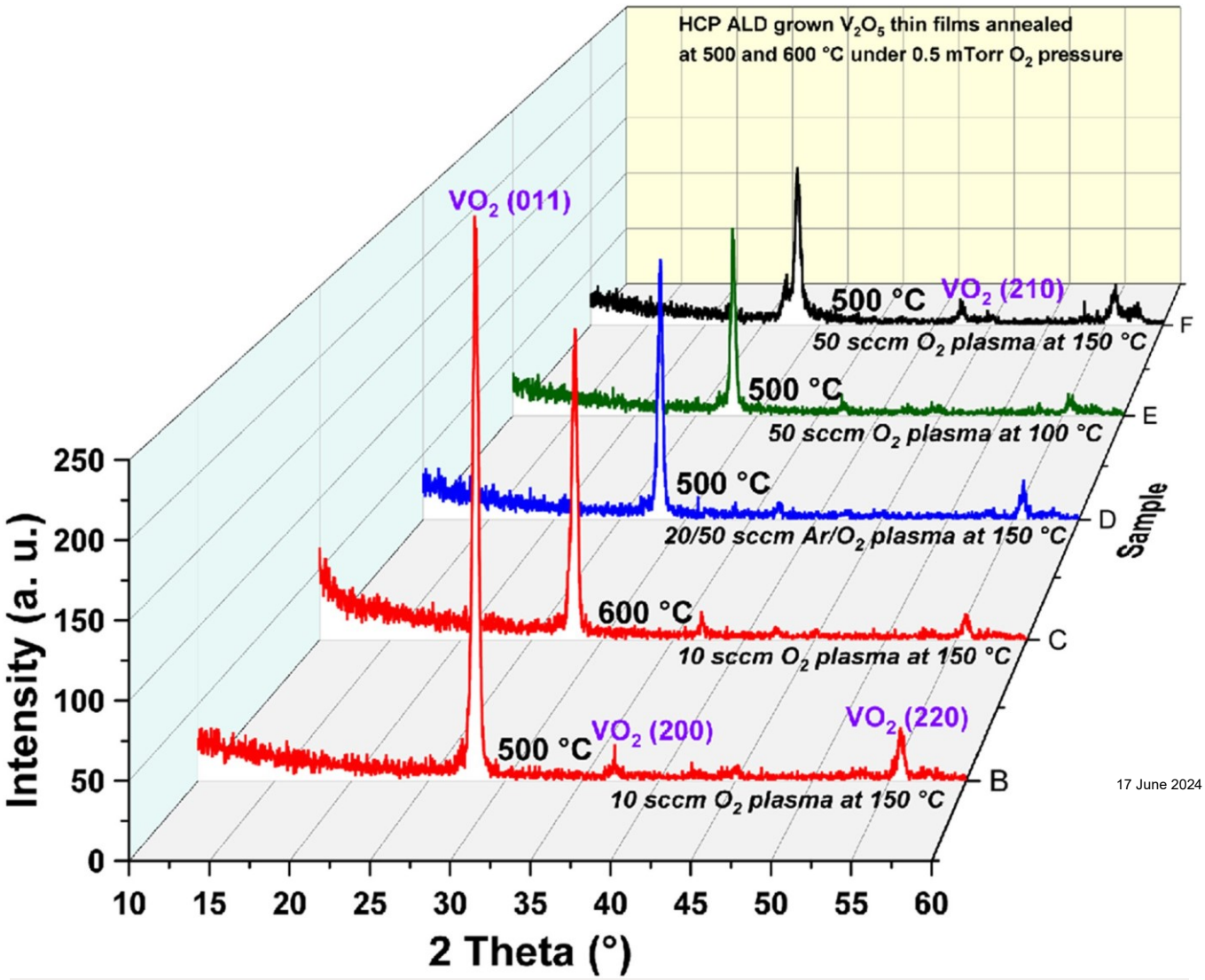




FIG. 12. GIXRD of ex situ postdeposition annealed HCP-ALD grown $V_2O_5$/Si(100) samples at 500 and 600 °C under 0.5 mTorr $O_2$ pressure resulting in the $VO_2$ state. The as-grown $V_2O_5$ was synthesized at 100 and 150 °C, 100 W, and various plasma gas flows.

TABLE IV. HCP-ALD grown $V_2O_5$ thin films by different plasma chemistries at 100 and 150 °C, and outcomes of postdeposition ex situ annealing on the selected $V_2O_5$ thin films under different annealing pressure and temperature.

| Selected samples | Plasma chemistries and growth temperatures of HCP-ALD grown $V_2O_5$ thin films | Annealing conditions: reactor pressure and temperature | | Transformed $VO_x$ phase |
|---|---|---|---|---|
| 1 | 50 SCCM $O_2$ plasma, 100 °C | 1 | 0.5 mTorr $O_2$ flow, 500 °C | $VO_2$ |
| 2 | 50 SCCM $O_2$ plasma, 150 °C | 2 | 0.5 mTorr $O_2$ flow, 600 °C | $VO_2$ |
| 3 | 10 SCCM $O_2$ plasma, 150 °C | | | |

FIG. 15. XRR analysis of 600-cycle HCP-ALD as-grown $VO_X$ thin films with 100 W $O_2$ (10 SCCM) plasma for 10 and 20 s plasma duration and in situ Ar plasma (100 W) annealed $V_2O_5$ thin films for 20 s. The Ar-plasma in situ annealing step is added to HCP-ALD grown $V_2O_5$ film recipe (150 °C, 100 W, 50 SCCM $O_2$ plasma for 10 s). The solid line and dotted line represent measured and calculated XRR patterns, respectively.

4 20/50 SCCM Ar/$O_2$ plasma, 150 °C

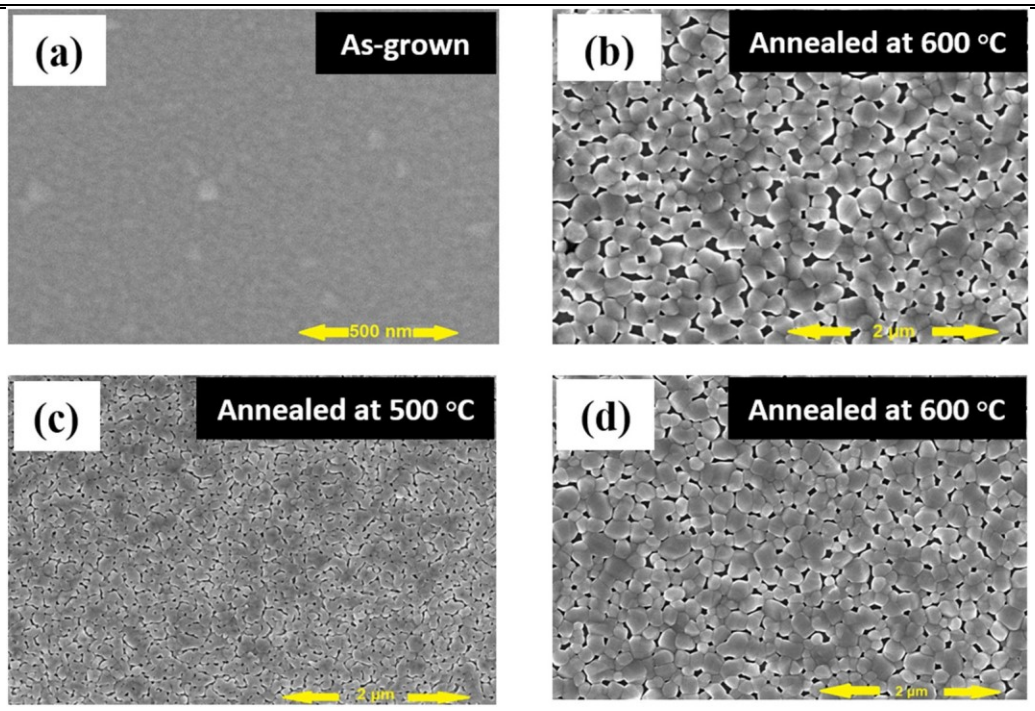

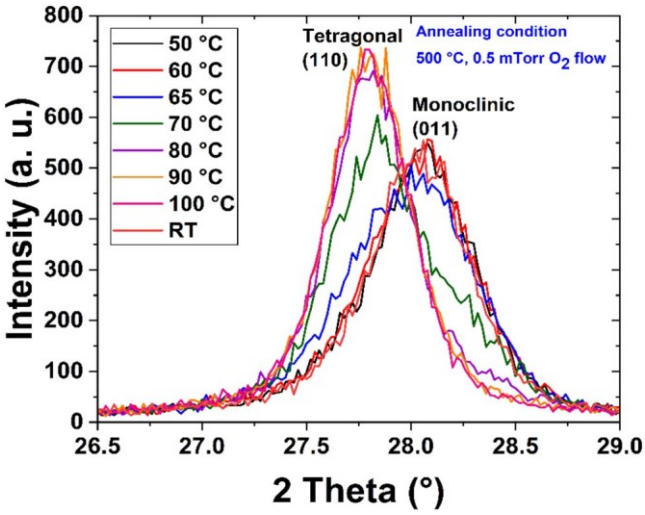


FIG. 13. Temperature dependent GIXRD measurement of the ex situ annealed $VO_2$ thin film samples showing crystalline phase transition from monoclinic to tetragonal $VO_2$ at a low temperature of ~70 °C. The temperature scan is performed from room temperature to 100 °C. The HCP-ALD grown $VO_x$ film is annealed at 500 °C under 0.5 mTorr $O_2$ pressure.

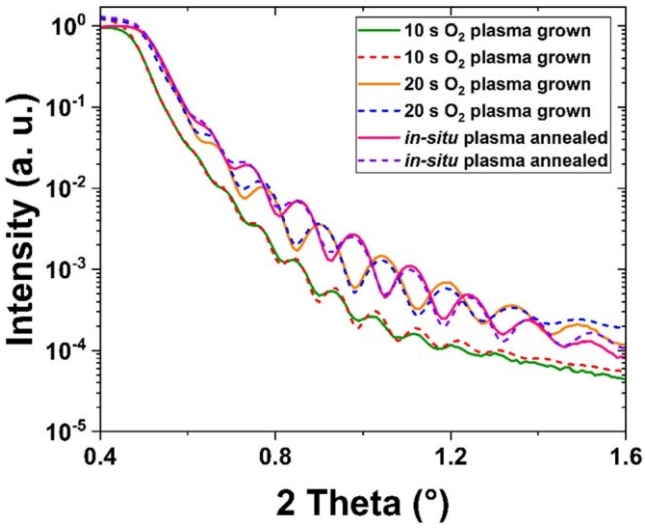


FIG. 14. HR-SEM images of the film surfaces from (a) HCP-ALD grown $V_2O_5$/Si (100) with 50 SCCM $O_2$-only plasma recipe, (b) 600 °C annealed $VO_2$ film (sample as-grown HCP-ALD condition: 50 SCCM $O_2$-only plasma), (c) 500 °C annealed $VO_2$ film with an as-grown condition of 10 SCCM $O_2$-only plasma, and (d) 600 °C annealed $VO_2$ film with 10 SCCM $O_2$-only plasma as-grown HCP-ALD recipe. The plasma power for HCP-ALD recipe is 100 W and postdeposition annealing is carried out at 0.5 mTorr $O_2$ pressure.

TABLE V. Film thickness, density, and surface roughness data extracted from XRR for 600 cycles 100 W HCP-ALD grown and in situ Ar-plasma annealed $VO_x$ thin films.

| Plasma chemistries and durations | Thickness (nm) by ex situ ellipsometry | Thickness (nm) by XRR | Density (g/cm$^3$) | Roughness (nm) |
|---|---|---|---|---|
| 10 SCCM only $O_2$ for 10 s | 75 | 83.35 | 2.85 | 3.16 |
| 10 SCCM only $O_2$ for 20 s | 48 | 53.35 | 3.19 | 2.48 |
| 20 SCCM Ar in situ plasma annealing for 20 s at 100 W | 50 | 59.13 | 3.07 | 2.17 |

The temperature-dependent resistivity measurement of the annealed $VO_2$ film is shown in Fig. 17. The $V_2O_5$ film (~155 nm) is grown on the 30 nm $Al_2O_3$ coated Si(100) substrate in the HCP-ALD reactor at 150 °C. The used plasma conditions are 20 s, 100 W, 10 SCCM $O_2$ flow. Postdeposition annealing is performed at 500 °C under 0.5 mTorr $O_2$ pressure, which converted $V_2O_5$ to $VO_2$ film. Then, 10 × 10 mm or 15 × 15 mm square-shaped van der Pauw (VdP) samples with soldered indium contacts at four corners are prepared for electrical characterization. The temperaturedependent resistivity measurement is carried out within a temperature range starting from room temperature (RT) to 130 °C. The resistivity measurement is performed in a customized Hall measurement setup for both heating (RT to 130 °C) and cooling (130 °C to RT) scans. Close to 2 orders



of magnitude change in

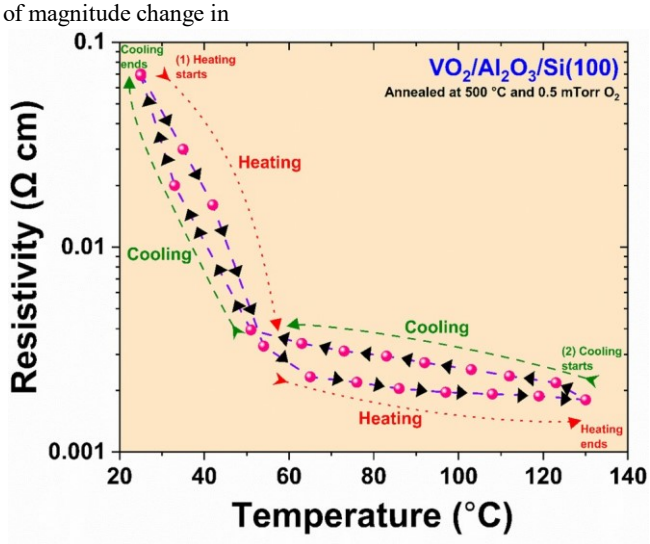

FIG. 17. Temperature-dependent resistivity measurement (both heating and cooling) of the annealed $VO_2$ thin film sample showing crystalline phase transition from monoclinic to tetragonal $VO_2$ around ~70 °C. The temperature scan is performed from room temperature up to 130 °C. For electrical insulation purpose, the HCP-ALD grown $VO_x$ film is grown on 30 nm $Al_2O_3$ coated Si(100) and is annealed at 500 °C under 0.5 mTorr $O_2$ pressure.

film resistivity has been observed, which relates to the transition from monoclinic $VO_2$ (high resistivity) to tetragonal $VO_2$ (low resistivity) phase around ~70 °C.[54] This behavior also conforms the temperature-dependent GIXRD scans, which indicated the phase transition at the same temperature. The cooling/reverse resistivity scan features a slight hysteresis characteristic.

## IV. CONCLUSIONS

We have studied the low-temperature ALD of crystalline $VO_x$ films using TEMAV metal precursor, various oxygen plasma gas mixtures, and two types of remote plasma sources: ICP and HCP. The difference between the ICP and HCP is in the plasma source configuration: the former is inductively coupled while the latter is capacitively coupled. Due to the plasma source configuration, the HCP is known to produce higher radical density. Comprehensive growth and material analyses using in situ and ex situ techniques as well as postdeposition annealing characteristics have been studied, which are not scrutinized yet to the best of our knowledge. Saturation curve studies were followed by longer runs for thicker films where substrate temperature, plasma parameters, and in situ Ar-annealing process are investigated. The resulting as-grown and annealed crystalline $VO_x$ films are characterized for their structural, optical, chemical, and electrical properties.

Both HCP-ALD and ICP-ALD techniques achieved as-grown crystalline $V_2O_5$ films at 150 °C substrate temperature. However, HCP-ALD showed significantly a higher GPC value (1.80 vs 0.64 Å) and a higher refractive index (2.76 vs 2.55). Both types of plasma sources and reactors successfully produced as-grown crystalline $V_2O_5$ film without needing any ex situ postdeposition annealing, which was not observed in the widely reported thermal-ALD grown $VO_x$ films. Prior ALD-grown $VO_x$ films extensively reported as-grown amorphous $VO_x$ layers that required postdeposition annealing processes at elevated temperatures for crystallization. This result confirms the positive impact of both types of plasma sources in achieving crystalline films at low substrate temperatures.

Ar-plasma in situ annealing and various growth conditions including substrate temperature variation, different plasma chemistries, and changing rf-plasma power during HCP-ALD experiments have also resulted in crystalline $V_2O_5$ with certain variations in pronounced diffraction peak intensities and GPC values. Hence, the incorporation of in situ Ar-plasma annealing in TEMAV and $O_2$ plasma recipes has not produced a notable crystalline improvement or change in the $VO_x$ crystal phase (i.e., from $V_2O_5$ to $VO_2$), though the linearity in the film thickness gain profile got noticeably enhanced.

While the as-grown film at 150 °C (optimized substrate temperature) was $V_2O_5$, the ex situ postdeposition annealing at 500 °C and 0.5 mTorr $O_2$ pressure has successfully transformed the film into polycrystalline $VO_2$ films. The temperature-dependent GIXRD and resistivity measurements have successfully confirmed the lowtemperature (~70 °C) metal-to-insulator phase transition (MIT) property of the achieved $VO_2$ layers.

In summary, crystalline $V_2O_5$ thin films are grown successfully using oxygen plasmas in both HCP-ALD and ICP-



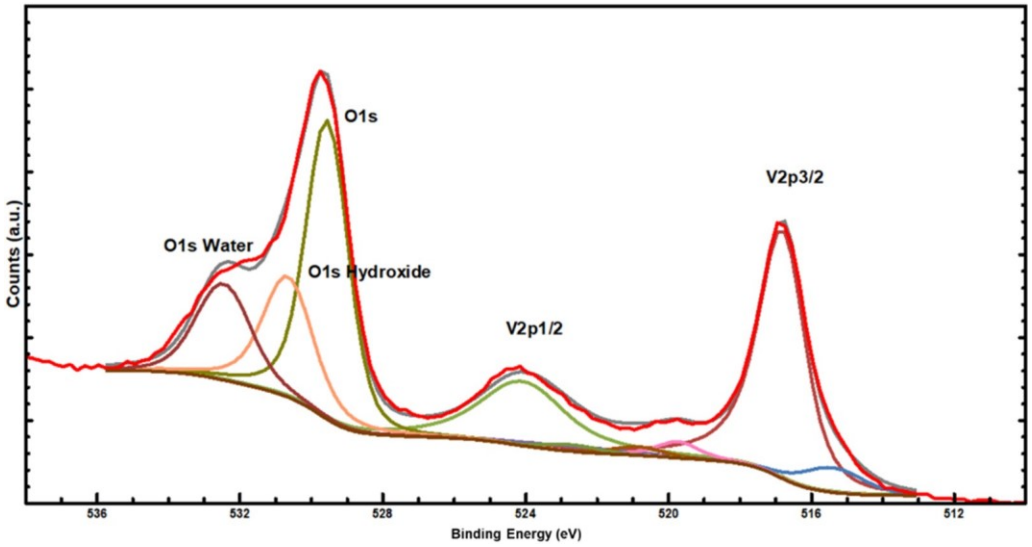


FIG. 16. HR-XPS O 1s and V 2p spectra of the $V_2O_5$ thin film grown by HCP-ALD at 100 W, 20 s 10 SCCM $O_2$-only plasma at 150 °C.

ALD reactors at a low substrate temperature of 150 °C. We have monitored the thin film growth surface reactions in the HCP-ALD reactor via real-time in situ ellipsometry. Postdeposition annealing processes under low $O_2$ pressure have demonstrated the tunability of the $V_2O_5$ film phase and formed $VO_2$ upon annealing at 500 °C and 0.5 mTorr $O_2$ pressure. The nearly two orders of magnitude resistivity drop around 70 °C can potentially be further increased by fine-tuning of the growth and annealing experiments. Furthermore, in situ Ar-plasma annealing process might be further investigated in a wider parameter space to achieve $V_2O_5$-to-$VO_2$ phase transition without needing a high-temperature postdeposition annealing process. Such an entirely low-temperature $VO_2$ synthesis could open new opportunities for this phase-change material toward electronic and optoelectronic device applications on low-temperature compatible substrates including cost-effective glass, polymer, and organic templates.

## ACKNOWLEDGMENTS

The authors would like to thank Daniela Morales and the support staff of the Institute of Materials Science (IMS) for their support in XRD measurements. The authors are also thankful to Ali Gokirmak and Helena Silva for their support in electrical measurements. This work was financially supported by the University of Connecticut, School of Engineering Startup Research Funding, the Research Excellence Program (REP) Grant supported by the University of Connecticut—Office of the Vice President for Research (OVPR) and GE Graduate Fellowship for Innovation, School of Engineering, University of Connecticut.

## AUTHOR DECLARATIONS Conflict of Interest

The authors have no conflicts to disclose.

### Author Contributions

Adnan Mohammad: Conceptualization (equal); Data curation (equal); Formal analysis (equal); Investigation (equal); Methodology (equal); Project administration (equal); Resources (equal); Software (equal); Validation (equal); Visualization (equal); Writing – original draft (equal); Writing – review & editing (equal). Krishna D. Joshi: Methodology (supporting); Visualization (supporting); Writing – review & editing (supporting). Dhan Rana: Methodology (supporting); Validation (supporting); Visualization (supporting); Writing – review & editing (supporting). Saidjafarzoda Ilhom: Methodology (supporting). Barrett Wells: Investigation (supporting); Writing – review & editing (supporting). Brian Willis: Investigation (supporting); Resources (supporting); Validation (supporting); Visualization (supporting); Writing – review & editing (supporting). Boris Sinkovic: Investigation (supporting); Methodology (supporting); Writing – review & editing (supporting). A. K. Okyay: Investigation (supporting); Writing – review & editing (supporting). Necmi Biyikli: Conceptualization (equal); Data curation (equal); Formal analysis (equal); Funding acquisition (equal); Investigation (equal); Methodology (equal); Project administration (equal); Resources (equal); Supervision (equal); Validation (equal); Visualization (equal); Writing – review & editing (equal).

## DATA AVAILABILITY

The data that support the findings of this study are available from the corresponding author upon reasonable request.

## REFERENCES

[1]S. M. George, Chem. Rev. 110, 111 (2010). [2]R. L. Puurunen, J. Appl. Phys. 97, 121301 (2005).
[3]H. Y. Shih, W. H. Lee, W. C. Kao, Y. C. Chuang, R. M. Lin, H. C. Lin, M. Shiojiri, and M. J. Chen, Sci. Rep. 7, 39717 (2017). [4]M. Alevli, C. Ozgit, I. Donmez, and N. Biyikli, J. Cryst. Growth 335, 51 (2011).
[5]M. Fang, H. Zhang, L. Sang, H. Cao, L. Yang, K. Ostrikov, I. Levchenko, and Q. Chen, Flexible Printed Electron. 2, 022001 (2017). [6]C. Ozgit-Akgun, E. Goldenberg, A. K. Okyay, and N. Biyikli, J. Mater. Chem. C 2, 2123 (2014). [7]J. Sheng, J. Park, D. W. Choi, J. Lim, and J. S. Park, ACS Appl. Mater. Interfaces 8, 31136 (2016).
[8]Z. Chen, H. Wang, X. Wang, P. Chen, Y. Liu, H. Zhao, Y. Zhao, and Y. Duan, Sci. Rep. 7, 40061 (2017).
[9]M. Alevli, C. Ozgit, I. Donmez, and N. Biyikli, Phys. Status Solidi A 209, 266 (2012). [10]J. A. van Delft, D. Garcia-Alonso, and W. M. M. Kessels, Semicond. Sci. Technol. 27, 074002 (2012).
[11]J. Schmidt, A. Merkle, R. Brendel, B. Hoex, M. C. M. van de Sanden, and W. M. M. Kessels, Prog. Photovoltaics Res. Appl. 16, 461 (2008). [12]M. Xie, X. Sun, C. Zhou, A. S. Cavanagh, H. Sun, T. Hu, G. Wang, J. Lian, and S. M. George, J. Electrochem. Soc. 162, A974 (2015). [13]Y. S. Jung, P. Lu, A. S. Cavanagh, C. Ban, G.-H. Kim, S.-H. Lee, S. M. George, S. J. Harris, and A. C. Dillon, Adv. Energy Mater. 3, 213 (2013). [14]A. Mohammad, S. Ilhom, D. Shukla, and N. Biyikli, J. Vac. Sci. Technol. A 40, 042401 (2022).
[15]B. J. O'Neill et al., ACS Catal. 5, 1804 (2015). [16]J. Lu, J. W. Elam, and P. C. Stair, Acc. Chem. Res. 46, 1806 (2013).
[17]M. A. Khalily, H. Eren, S. Akbayrak, H. H. Susapto, N. Biyikli, S. Özkar, and M. O. Guler, Angew. Chem. Int. Ed. 55, 12257 (2016).
[18]A. Richter, J. Benick, M. Hermle, and S. W. Glunz, Phys. Status Solidi RRL 5, 202 (2011). [19]A. Mohammad, D. Shukla, S. Ilhom, B. Willis, B. Johs, A. K. Okyay, and N. Biyikli, J. Vac. Sci. Technol. A 37, 020927 (2019).
[20]B. J. Kim et al., Energy Environ. Sci. 8, 916 (2015).
[21]J. Sheng, K.-L. Han, T. H. Hong, W.-H. Choi, and J.-S. Park, J. Semicond. 39, 011008 (2018). [22]A. Mohammad, D. Shukla, S. Ilhom, B. Willis, A. K. Okyay, and N. Biyikli, Int. J. High Speed Electron. Syst. 28, 1940020 (2019).
[23]Y. Liu, M. Clark, Q. Zhang, D. Yu, D. Liu, J. Liu, and G. Cao, Adv. Energy Mater. 1, 194 (2011).

[24]K. Schneider, M. Lubecka, and A. Czapla, Sens. Actuators, B 236, 970 (2016).
[25]M. Li et al., AIP Adv. 12, 055203 (2022).
[26]M. Tian, R. Li, C. Liu, D. Long, and G. Cao, ACS Appl. Mater. Interfaces 11, 15573 (2019). [27]Q. Meng, K. Cai, Y. Chen, and L. Chen, Nano Energy 36, 268 (2017).
[28]S. D. Perera, B. Patel, J. Bonso, M. Grunewald, J. P. Ferraris, and K. J. Balkus, Jr., ACS Appl. Mater. Interfaces 3, 4512 (2017). [29]J. Yang, T. Lan, J. Liu, Y. Song, and M. Wei, Electrochim. Acta 105, 489 (2013).
[30]Y. Zhang, J. Zheng, Y. Zhao, T. Hu, Z. Gao, and C. Meng, Appl. Surf. Sci. 377, 385 (2016). [31]M. Panagopoulou, D. Vernardou, E. Koudoumas, N. Katsarakis, D. Tsoukalas, and Y. S. Raptis, J. Phys. Chem. C 121, 70 (2017).
[32]A. M. Andersson, C. G. Granqvist, and J. R. Stevens, Appl. Opt. 28, 3295 (1989).
[33]D. T. Gillaspie, R. C. Tenent, and A. C. Dillon, J. Mater. Chem. 20, 9585 (2010). [34]G. Stefanovich, A. Pergament, and D. Stefanovich, J. Phys.: Condens. Matter 12, 8837 (2000). [35]L. A. Gea and L. A. Boatner, Appl. Phys. Lett. 68, 3081 (1996).
[36]C. G. Granqvist, P. C. Lansåker, N. R. Mlyuka, G. A. Niklasson, and E. Avendaño, Sol. Energy Mater. Sol. Cells 93, 2032 (2009).
[37]C. G. Granqvist, S. Green, G. A. Niklasson, N. R. Mlyuka, S. von Kræmer, and P. Georén, Thin Solid Films 518, 3046 (2010).
[38]T. Driscoll et al., Appl. Phys. Lett. 93, 024101 (2008). [39]T. Driscoll et al., Science 325, 1518 (2009).
[40]P. A. Premkumar, M. Toeller, I. P. Radu, C. Adelmann, M. Schaekers, J. Meersschaut, T. Conard, and S. V. Elshocht, ECS J. Solid State Sci. Technol. 1, P169 (2012). [41]X. Wang, Z. Guo, Y. Gao, and J. Wang, J. Mater. Res. 32, 37 (2017).
[42]V. P. Prasadam, B. Dey, S. Bulou, T. Schenk, and N. Bahlawane, Mater. Today Chem. 12, 332 (2019). [43]J. Musschoot, D. Deduytsche, H. Poelman, J. Haemers, R. L. Van Meirhaeghe, S. Van den Berghe, and C. Detavernier, J. Electrochem. Soc. 156, P122 (2009).
[44]I. I. Kazadojev, Growth of $V_2O_5$ Films for Electrochromic and Battery Applications (The National University of Ireland, Cork, 2018). [45]K. Schneider, J. Mater. Sci.: Mater. Electron. 31, 10478 (2020).
[46]J. Musschoot, D. Deduytsche, H. Poelman, J. Haemers, R. Vanmeirhaeghe, S. Van den Berghe, and C. Detavernier, J. Electrochem. Soc. 156, P122 (2009). [47]Q. Shi, W. Huang, J. Yan, Y. Zhang, M. Mao, Y. Zhang, Y. Xu, and Y. Zhang, J. Sol-Gel Sci. Technol. 59, 591 (2011).
[48]S. H. Lee, P. Liu, and C. E. Tracy, Electrochem. Solid-State Lett. 6, A275 (2003). [49]Z. Tarnawski, K. Zakrzewska, N. T. H. Kim-Ngan, M. Krupska, S. Sowa, K. Drogowska, L. Havela, and A. G. Balogh, Acta Phys. Pol. A 128, 431 (2015).
[50]W. C. Kao, W. H. Lee, S. H. Yi, T. H. Shen, H. C. L. and M, and J. Chen, RSC Adv. 9, 12226 (2019).
[51]G. Y. Song, C. Oh, S. Sinha, J. Son, and J. Heo, ACS Appl. Mater. Interfaces 9, 23909 (2017). [52]T. Cottre, M. Fingerle, M. Kranz, T. Mayer, B. Kaiser, and W. Jaegermann, Adv. Mater. Interfaces 8, 2002257 (2021).
[53]H. S. Casalongue, S. Kaya, V. Viswanathan, D. J. Miller, D. Friebel, H. A. Hansen, J. K. Nørskov, A. Nilsson, and H. Ogasawara, Nat Commun. 4, 2817 (2013).
[54]Y. Zhang, W. Xiong, W. Chen, and Y. Zheng, Nanomaterials 11, 338 (2021). [55]See supplementary material at https://www.scitation.org/doi/suppl/10.1116/6.0002383 for real-time in situ ellipsometry recorded 150 cycles HCP-ALD grown $VO_x$ thin film thickness data at 100, 150, 200, and 250 °C.